

A search for extremely-high-energy neutrinos and first constraints on the ultra-high-energy cosmic-ray proton fraction with IceCube

R. Abbasi,¹⁷ M. Ackermann,⁶⁵ J. Adams,¹⁸ S. K. Agarwalla,^{40,*} J. A. Aguilar,¹¹ M. Ahlers,²² J.M. Alameddine,²³ N. M. Amin,⁴⁴ K. Andeen,⁴² C. Argüelles,¹⁴ Y. Ashida,⁵³ S. Athanasiadou,⁶⁵ S. N. Axani,⁴⁴ R. Babu,²⁴ X. Bai,⁵⁰ A. Balagopal V.,⁴⁰ M. Baricevic,⁴⁰ S. W. Barwick,³⁰ S. Bash,²⁷ V. Basu,⁴⁰ R. Bay,⁷ J. J. Beatty,^{20,21} J. Becker Tjus,^{10,†} J. Beise,⁶³ C. Bellenghi,²⁷ S. BenZvi,⁵² D. Berley,¹⁹ E. Bernardini,⁴⁸ D. Z. Besson,³⁶ E. Blaufuss,¹⁹ L. Bloom,⁶⁰ S. Blot,⁶⁵ F. Bontempo,³¹ J. Y. Book Motzkin,¹⁴ C. Boscolo Meneguolo,⁴⁸ S. Böser,⁴¹ O. Botner,⁶³ J. Böttcher,¹ J. Braun,⁴⁰ B. Brinson,⁵ Z. Brisson-Tsavoussis,³³ J. Brostean-Kaiser,⁶⁵ L. Brusa,¹ R. T. Burley,² D. Butterfield,⁴⁰ M. A. Campana,⁴⁹ I. Caracas,⁴¹ K. Carloni,¹⁴ J. Carpio,^{34,35} S. Chattopadhyay,^{40,*} N. Chau,¹¹ Z. Chen,⁵⁶ D. Chirkin,⁴⁰ S. Choi,^{57,58} B. A. Clark,¹⁹ A. Coleman,⁶³ P. Coleman,¹ G. H. Collin,¹⁵ A. Connolly,^{20,21} J. M. Conrad,¹⁵ R. Corley,⁵³ D. F. Cowen,^{61,62} C. De Clercq,¹² J. J. DeLaunay,⁶⁰ D. Delgado,¹⁴ S. Deng,¹ A. Desai,⁴⁰ P. Desiati,⁴⁰ K. D. de Vries,¹² G. de Wasseige,³⁷ T. DeYoung,²⁴ A. Diaz,¹⁵ J. C. Díaz-Vélez,⁴⁰ P. Dierichs,¹ M. Dittmer,⁴³ A. Domi,²⁶ L. Draper,⁵³ H. Dujmovic,⁴⁰ D. Durnford,²⁵ K. Dutta,⁴¹ M. A. DuVernois,⁴⁰ T. Ehrhardt,⁴¹ L. Eidenschink,²⁷ A. Eimer,²⁶ P. Eller,²⁷ E. Ellinger,⁶⁴ S. El Mentawi,¹ D. Elsässer,²³ R. Engel,^{31,32} H. Erpenbeck,⁴⁰ W. Esmail,⁴³ J. Evans,¹⁹ P. A. Evenson,⁴⁴ K. L. Fan,¹⁹ K. Fang,⁴⁰ K. Farrag,¹⁶ A. R. Fazely,⁶ A. Fedynitch,⁵⁹ N. Feigl,⁹ S. Fiedlschuster,²⁶ C. Finley,⁵⁵ L. Fischer,⁶⁵ D. Fox,⁶¹ A. Franckowiak,¹⁰ S. Fukami,⁶⁵ P. Fürst,¹ J. Gallagher,³⁹ E. Ganster,¹ A. Garcia,¹⁴ M. Garcia,⁴⁴ G. Garg,^{40,*} E. Genton,^{14,37} L. Gerhardt,⁸ A. Ghadimi,⁶⁰ C. Girard-Carillo,⁴¹ C. Glaser,⁶³ T. Glüsenskamp,⁶³ J. G. Gonzalez,⁴⁴ S. Goswami,^{34,35} A. Granados,²⁴ D. Grant,¹³ S. J. Gray,¹⁹ S. Griffin,⁴⁰ S. Griswold,⁵² K. M. Groth,²² D. Guevel,⁴⁰ C. Günther,¹ P. Gutjahr,²³ C. Ha,⁵⁴ C. Haack,²⁶ A. Hallgren,⁶³ L. Halve,¹ F. Halzen,⁴⁰ L. Hamacher,¹ H. Hamdaoui,⁵⁶ M. Ha Minh,²⁷ M. Handt,¹ K. Hanson,⁴⁰ J. Hardin,¹⁵ A. A. Harnisch,²⁴ P. Hatch,³³ A. Haungs,³¹ J. Häußler,¹ K. Helbing,⁶⁴ J. Hellrung,¹⁰ J. Hermannsgabner,¹ L. Heuermann,¹ N. Heyer,⁶³ S. Hickford,⁶⁴ A. Hidvegi,⁵⁵ C. Hill,¹⁶ G. C. Hill,² R. Hmaid,¹⁶ K. D. Hoffman,¹⁹ S. Hori,⁴⁰ K. Hoshina,^{40,‡} M. Hostert,¹⁴ W. Hou,³¹ T. Huber,³¹ K. Hultqvist,⁵⁵ M. Hünnefeld,⁴⁰ R. Hussain,⁴⁰ K. Hyon,^{23,59} A. Ishihara,¹⁶ W. Iwakiri,¹⁶ M. Jacquart,⁴⁰ S. Jain,⁴⁰ O. Janik,²⁶ M. Jansson,⁵⁷ M. Jeong,⁵³ M. Jin,¹⁴ B. J. P. Jones,⁴ N. Kamp,¹⁴ D. Kang,³¹ W. Kang,⁵⁷ X. Kang,⁴⁹ A. Kappes,⁴³ D. Kappesser,⁴¹ L. Kardum,²³ T. Karg,⁶⁵ M. Karl,²⁷ A. Karle,⁴⁰ A. Katil,²⁵ U. Katz,²⁶ M. Kauer,⁴⁰ J. L. Kelley,⁴⁰ M. Khanal,⁵³ A. Khatee Zathul,⁴⁰ A. Kheirandish,^{34,35} J. Kiryluk,⁵⁶ S. R. Klein,^{7,8} Y. Kobayashi,¹⁶ A. Kochocki,²⁴ R. Koirala,⁴⁴ H. Kolanoski,⁹ T. Kontrimas,²⁷ L. Köpke,⁴¹ C. Kopper,²⁶ D. J. Koskinen,²² P. Koundal,⁴⁴ M. Kowalski,^{9,65} T. Kozyrnets,²² N. Krieger,¹⁰ J. Krishnamoorthi,^{40,*} T. Krishnan,¹⁴ K. Kruiswijk,³⁷ E. Krupczak,²⁴ A. Kumar,⁶⁵ E. Kun,¹⁰ N. Kurahashi,⁴⁹ N. Lad,⁶⁵ C. Lagunas Gualda,²⁷ M. Lamoureux,³⁷ M. J. Larson,¹⁹ F. Lauber,⁶⁴ J. P. Lazar,³⁷ K. Leonard DeHolton,⁶² A. Leszczyńska,⁴⁴ J. Liao,⁵ M. Lincetto,¹⁰ Y. T. Liu,⁶² M. Liubarska,²⁵ C. Love,⁴⁹ L. Lu,⁴⁰ F. Lucarelli,²⁸ W. Luszczak,^{20,21} Y. Lyu,^{7,8} J. Madsen,⁴⁰ E. Magnus,¹² K. B. M. Mahn,²⁴ Y. Makino,⁴⁰ E. Manao,²⁷ S. Mancina,⁴⁸ A. Mand,⁴⁰ W. Marie Sainte,⁴⁰ I. C. Mariş,¹¹ S. Marka,⁴⁶ Z. Marka,⁴⁶ M. Marsee,⁶⁰ I. Martinez-Soler,¹⁴ R. Maruyama,⁴⁵ F. Mayhew,²⁴ F. McNally,³⁸ J. V. Mead,²² K. Meagher,⁴⁰ S. Mechbal,⁶⁵ A. Medina,²¹ M. Meier,¹⁶ Y. Merckx,¹² L. Merten,¹⁰ J. Mitchell,⁶ T. Montaruli,²⁸ R. W. Moore,²⁵ Y. Morii,¹⁶ R. Morse,⁴⁰ M. Moulai,⁴⁰ T. Mukherjee,³¹ R. Naab,⁶⁵ M. Nakos,⁴⁰ U. Naumann,⁶⁴ J. Necker,⁶⁵ A. Negi,⁴ L. Neste,⁵⁵ M. Neumann,⁴³ H. Niederhausen,²⁴ M. U. Nisa,²⁴ K. Noda,¹⁶ A. Noell,¹ A. Novikov,⁴⁴ A. Obertacke Pollmann,¹⁶ V. O'Dell,⁴⁰ A. Olivas,¹⁹ R. Orsoe,²⁷ J. Osborn,⁴⁰ E. O'Sullivan,⁶³ V. Palusova,⁴¹ H. Pandya,⁴⁴ N. Park,³³ G. K. Parker,⁴ V. Parrish,²⁴ E. N. Paudel,⁴⁴ L. Paul,⁵⁰ C. Pérez de los Heros,⁶³ T. Pernice,⁶⁵ J. Peterson,⁴⁰ A. Pizzuto,⁴⁰ M. Plum,⁵⁰ A. Pontén,⁶³ Y. Popovych,⁴¹ M. Prado Rodriguez,⁴⁰ B. Pries,²⁴ R. Procter-Murphy,¹⁹ G. T. Przybylski,⁸ L. Pyras,⁵³ C. Raab,³⁷ J. Rack-Helleis,⁴¹ N. Rad,⁶⁵ M. Ravn,⁶³ K. Rawlins,³ Z. Rechav,⁴⁰ A. Rehman,⁴⁴ E. Resconi,²⁷ S. Reusch,⁶⁵ W. Rhode,²³ B. Riedel,⁴⁰ A. Rifaie,⁶⁴ E. J. Roberts,² S. Robertson,^{7,8} S. Rodan,^{57,58} M. Rongen,²⁶ A. Rosted,¹⁶ C. Rott,^{53,57} T. Ruhe,²³ L. Ruohan,²⁷ D. Ryckbosch,²⁹ I. Safa,⁴⁰ J. Saffer,³² D. Salazar-Gallegos,²⁴ P. Sampathkumar,³¹ A. Sandroock,⁶⁴ M. Santander,⁶⁰ S. Sarkar,²⁵ S. Sarkar,⁴⁷ J. Savelberg,¹ P. Savina,⁴⁰ P. Schaile,²⁷ M. Schaufel,¹ H. Schieler,³¹ S. Schindler,²⁶ L. Schlickmann,⁴¹ B. Schlüter,⁴³ F. Schlüter,¹¹ N. Schmeisser,⁶⁴ T. Schmidt,¹⁹ J. Schneider,²⁶ F. G. Schröder,^{31,44} L. Schumacher,²⁶ S. Schwirn,¹ S. Sclafani,¹⁹ D. Seckel,⁴⁴ L. Seen,⁴⁰ M. Seikh,³⁶ M. Seo,⁵⁷ S. Seunarine,⁵¹ P. Sevl Myhr,³⁷ R. Shah,⁴⁹ S. Shefali,³² N. Shimizu,¹⁶ M. Silva,⁴⁰ B. Skrzypek,⁷ B. Smithers,⁴ R. Snihur,⁴⁰ J. Soedingrekso,²³ A. Sogaard,²² D. Soldin,⁵³ P. Soldin,¹ G. Sommani,¹⁰ C. Spannfellner,²⁷ G. M. Spiczak,⁵¹ C. Spiering,⁶⁵ J. Stachurska,²⁹ M. Stamatikos,²¹ T. Stanev,⁴⁴ T. Stezelberger,⁸ T. Stürwald,⁶⁴ T. Stuttard,²² G. W. Sullivan,¹⁹ I. Taboada,⁵ S. Ter-Antonyan,⁶ A. Terliuk,²⁷ M.

Thiesmeyer,⁴⁰ W. G. Thompson,¹⁴ J. Thwaites,⁴⁰ S. Tilav,⁴⁴ K. Tollefson,²⁴ C. Tönnis,⁵⁷ S. Toscano,¹¹ D. Tosi,⁴⁰ A. Trettin,⁶⁵ M. A. Unland Elorrieta,⁴³ A. K. Upadhyay,^{40,*} K. Upshaw,⁶ A. Vaidyanathan,⁴² N. Valtonen-Mattila,⁶³ J. Vandenbroucke,⁴⁰ N. van Eijndhoven,¹² D. Vannerom,¹⁵ J. van Santen,⁶⁵ J. Vara,⁴³ F. Varsi,³² J. Veitch-Michaelis,⁴⁰ M. Venugopal,³¹ M. Vereecken,³⁷ S. Vergara Carrasco,¹⁸ S. Verpoest,⁴⁴ D. Veske,⁴⁶ A. Vijai,¹⁹ C. Walck,⁵⁵ A. Wang,⁵ C. Weaver,²⁴ P. Weigel,¹⁵ A. Weindl,³¹ J. Weldert,⁶² A. Y. Wen,¹⁴ C. Wendt,⁴⁰ J. Werthebach,²³ M. Weyrauch,³¹ N. Whitehorn,²⁴ C. H. Wiebusch,¹ D. R. Williams,⁶⁰ L. Witthaus,²³ M. Wolf,²⁷ G. Wrede,²⁶ X. W. Xu,⁶ J. P. Yanez,²⁵ E. Yildizci,⁴⁰ S. Yoshida,¹⁶ R. Young,³⁶ F. Yu,¹⁴ S. Yu,⁵³ T. Yuan,⁴⁰ A. Zegarelli,¹⁰ S. Zhang,²⁴ Z. Zhang,⁵⁶ P. Zhelnin,¹⁴ P. Zilberman,⁴⁰ and M. Zimmerman⁴⁰

(IceCube Collaboration)

¹*III. Physikalisches Institut, RWTH Aachen University, D-52056 Aachen, Germany*

²*Department of Physics, University of Adelaide, Adelaide, 5005, Australia*

³*Dept. of Physics and Astronomy, University of Alaska Anchorage, 3211 Providence Dr., Anchorage, AK 99508, USA*

⁴*Dept. of Physics, University of Texas at Arlington, 502 Yates St., Science Hall Rm 108, Box 19059, Arlington, TX 76019, USA*

⁵*School of Physics and Center for Relativistic Astrophysics, Georgia Institute of Technology, Atlanta, GA 30332, USA*

⁶*Dept. of Physics, Southern University, Baton Rouge, LA 70813, USA*

⁷*Dept. of Physics, University of California, Berkeley, CA 94720, USA*

⁸*Lawrence Berkeley National Laboratory, Berkeley, CA 94720, USA*

⁹*Institut für Physik, Humboldt-Universität zu Berlin, D-12489 Berlin, Germany*

¹⁰*Fakultät für Physik & Astronomie, Ruhr-Universität Bochum, D-44780 Bochum, Germany*

¹¹*Université Libre de Bruxelles, Science Faculty CP230, B-1050 Brussels, Belgium*

¹²*Vrije Universiteit Brussel (VUB), Dienst ELEM, B-1050 Brussels, Belgium*

¹³*Dept. of Physics, Simon Fraser University, Burnaby, BC V5A 1S6, Canada*

¹⁴*Department of Physics and Laboratory for Particle Physics and Cosmology, Harvard University, Cambridge, MA 02138, USA*

¹⁵*Dept. of Physics, Massachusetts Institute of Technology, Cambridge, MA 02139, USA*

¹⁶*Dept. of Physics and The International Center for Hadron Astrophysics, Chiba University, Chiba 263-8522, Japan*

¹⁷*Department of Physics, Loyola University Chicago, Chicago, IL 60660, USA*

¹⁸*Dept. of Physics and Astronomy, University of Canterbury, Private Bag 4800, Christchurch, New Zealand*

¹⁹*Dept. of Physics, University of Maryland, College Park, MD 20742, USA*

²⁰*Dept. of Astronomy, Ohio State University, Columbus, OH 43210, USA*

²¹*Dept. of Physics and Center for Cosmology and Astro-Particle Physics, Ohio State University, Columbus, OH 43210, USA*

²²*Niels Bohr Institute, University of Copenhagen, DK-2100 Copenhagen, Denmark*

²³*Dept. of Physics, TU Dortmund University, D-44221 Dortmund, Germany*

²⁴*Dept. of Physics and Astronomy, Michigan State University, East Lansing, MI 48824, USA*

²⁵*Dept. of Physics, University of Alberta, Edmonton, Alberta, T6G 2E1, Canada*

²⁶*Erlangen Centre for Astroparticle Physics, Friedrich-Alexander-Universität Erlangen-Nürnberg, D-91058 Erlangen, Germany*

²⁷*Physik-department, Technische Universität München, D-85748 Garching, Germany*

²⁸*Département de physique nucléaire et corpusculaire, Université de Genève, CH-1211 Genève, Switzerland*

²⁹*Dept. of Physics and Astronomy, University of Gent, B-9000 Gent, Belgium*

³⁰*Dept. of Physics and Astronomy, University of California, Irvine, CA 92697, USA*

³¹*Karlsruhe Institute of Technology, Institute for Astroparticle Physics, D-76021 Karlsruhe, Germany*

³²*Karlsruhe Institute of Technology, Institute of Experimental Particle Physics, D-76021 Karlsruhe, Germany*

³³*Dept. of Physics, Engineering Physics, and Astronomy, Queen's University, Kingston, ON K7L 3N6, Canada*

³⁴*Department of Physics & Astronomy, University of Nevada, Las Vegas, NV 89154, USA*

³⁵*Nevada Center for Astrophysics, University of Nevada, Las Vegas, NV 89154, USA*

³⁶*Dept. of Physics and Astronomy, University of Kansas, Lawrence, KS 66045, USA*

³⁷*Centre for Cosmology, Particle Physics and Phenomenology - CP3, Université catholique de Louvain, Louvain-la-Neuve, Belgium*

³⁸*Department of Physics, Mercer University, Macon, GA 31207-0001, USA*

³⁹*Dept. of Astronomy, University of Wisconsin—Madison, Madison, WI 53706, USA*

⁴⁰*Dept. of Physics and Wisconsin IceCube Particle Astrophysics Center, University of Wisconsin—Madison, Madison, WI 53706, USA*

⁴¹*Institute of Physics, University of Mainz, Staudinger Weg 7, D-55099 Mainz, Germany*

⁴²*Department of Physics, Marquette University, Milwaukee, WI 53201, USA*

⁴³*Institut für Kernphysik, Universität Münster, D-48149 Münster, Germany*

- ⁴⁴*Bartol Research Institute and Dept. of Physics and Astronomy,
University of Delaware, Newark, DE 19716, USA*
- ⁴⁵*Dept. of Physics, Yale University, New Haven, CT 06520, USA*
- ⁴⁶*Columbia Astrophysics and Nevis Laboratories,
Columbia University, New York, NY 10027, USA*
- ⁴⁷*Dept. of Physics, University of Oxford, Parks Road, Oxford OX1 3PU, United Kingdom*
- ⁴⁸*Dipartimento di Fisica e Astronomia Galileo Galilei,
Università Degli Studi di Padova, I-35122 Padova PD, Italy*
- ⁴⁹*Dept. of Physics, Drexel University, 3141 Chestnut Street, Philadelphia, PA 19104, USA*
- ⁵⁰*Physics Department, South Dakota School of Mines and Technology, Rapid City, SD 57701, USA*
- ⁵¹*Dept. of Physics, University of Wisconsin, River Falls, WI 54022, USA*
- ⁵²*Dept. of Physics and Astronomy, University of Rochester, Rochester, NY 14627, USA*
- ⁵³*Department of Physics and Astronomy, University of Utah, Salt Lake City, UT 84112, USA*
- ⁵⁴*Dept. of Physics, Chung-Ang University, Seoul 06974, Republic of Korea*
- ⁵⁵*Oskar Klein Centre and Dept. of Physics, Stockholm University, SE-10691 Stockholm, Sweden*
- ⁵⁶*Dept. of Physics and Astronomy, Stony Brook University, Stony Brook, NY 11794-3800, USA*
- ⁵⁷*Dept. of Physics, Sungkyunkwan University, Suwon 16419, Republic of Korea*
- ⁵⁸*Institute of Basic Science, Sungkyunkwan University, Suwon 16419, Republic of Korea*
- ⁵⁹*Institute of Physics, Academia Sinica, Taipei, 11529, Taiwan*
- ⁶⁰*Dept. of Physics and Astronomy, University of Alabama, Tuscaloosa, AL 35487, USA*
- ⁶¹*Dept. of Astronomy and Astrophysics, Pennsylvania State University, University Park, PA 16802, USA*
- ⁶²*Dept. of Physics, Pennsylvania State University, University Park, PA 16802, USA*
- ⁶³*Dept. of Physics and Astronomy, Uppsala University, Box 516, SE-75120 Uppsala, Sweden*
- ⁶⁴*Dept. of Physics, University of Wuppertal, D-42119 Wuppertal, Germany*
- ⁶⁵*Deutsches Elektronen-Synchrotron DESY, Platanenallee 6, D-15738 Zeuthen, Germany*
- (Dated: Feb 4th 2025)

We present a search for the diffuse extremely-high-energy neutrino flux using 12.6 years of IceCube data. The non-observation of neutrinos with energies well above 10 PeV constrains the all-flavor neutrino flux at 10^{18} eV to a level of $E^2\Phi_{\nu_e+\nu_\mu+\nu_\tau} \simeq 10^{-8}$ GeV cm⁻² s⁻¹ sr⁻¹, the most stringent limit to date. Using this data, we constrain the proton fraction of ultra-high-energy cosmic rays (UHECRs) above $\simeq 30$ EeV to be $\lesssim 70\%$ (at 90% CL) if the cosmological evolution of the sources is comparable to or stronger than the star formation rate. This result complements direct air-shower measurements by being insensitive to uncertainties associated with hadronic interaction models. It is the first such result to disfavor the “proton-only” hypothesis for UHECRs using neutrino data.

Introduction — Extremely-high-energy neutrinos (EHE ν , $E_\nu \gtrsim 10^{16}$ eV = 10 PeV) are unique messengers of the distant universe. Unlike photons and ultra-high-energy cosmic rays (UHECRs, $E_{\text{CR}} \geq 10^{18}$ eV = 1 EeV), neutrinos are chargeless and only weakly interacting, allowing them to travel undeflected by magnetic fields and unattenuated by interactions with background photons. Their fluxes are closely linked to the properties of UHECR sources, which remain unidentified [1, 2]. Of particular interest is the chemical composition of UHECRs, which carries more information about the source environments than spectral measurements. Inside source environments, UHECRs can interact with ambient photon fields and matter, producing *astrophysical neutrinos* carrying up to $\sim 5\%$ of the parent cosmic ray energy. Additionally, after escaping their sources, UHECRs can interact with the cosmic microwave background (CMB) and extragalactic background light (EBL), creating a flux of *cosmogenic neutrinos* [3–20]. Interactions with the CMB are presumed responsible for the “GZK-cutoff” of extragalactic UHECRs [21, 22] above $\sim 10^{19.6}$ eV. The production of cosmogenic neutrinos depends on a few key features of UHECR sources: their composition, spectrum, and distribution as function of redshift. Thus, the measurement or even non-observation of cosmogenic neutrinos can constrain some of these features.

In this Letter, we report a search for EHE ν using 12.6 years of data from the IceCube Neutrino Observatory. The data was taken between June 2010 and June 2023, corresponding to 4605 days of livetime. This is 50% more exposure than that of the previous IceCube search [23]. Additionally, the event selection has been re-optimized, improving the effective area by $\sim 15\%$ near 1 EeV. The null observation of cosmogenic neutrinos places significant constraints on the cosmological evolution of UHECR sources and, moreover, the composition of UHECRs. In this work, we investigate the specific hypothesis of a proton-only composition of UHECRs with the GZK-cutoff generating the observed suppression of UHECRs at EeV energies. The method was proposed in [9], and in a similar fashion applied to the neutrino measurement by the Pierre Auger collaboration [24]. We find, at 90% CL, that the observed fraction of UHECRs that are protons at Earth above $\simeq 30$ EeV cannot exceed 70% if the source evolution is comparable to the star formation rate (SFR) — a general tracer of matter density in the Universe. These constraints are complementary to, and agree with, direct air-shower measurements [25, 26] by being insensitive to uncertainties associated with hadronic interaction models.

Data Sample — IceCube [27] is a neutrino detector at the South Pole. It consists of 5160 Digital Optical Modules (DOMs), distributed on 86 strings, instrumenting a cubic kilometer of ice at depths between 1450 m and 2450 m. Each DOM hosts a 10-inch photomultiplier tube [28] and readout electronics [29].

Charged particles produced in neutrino interactions give rise to Cherenkov light when propagating through the ice. Those Cherenkov photons are detected by DOMs and converted into photoelectrons (PE). On top of the IceCube strings, a surface array called IceTop [30] measures cosmic-ray air showers. EHE ν events in IceCube are observed as either tracks — light depositions along the trajectory of a long-range μ/τ produced in ν_μ/ν_τ charged-current interactions — or cascades — approximately spherical light depositions arising from all-flavor neutral-current interactions and charged-current interactions of ν_e .

This search aims to select cosmogenic neutrinos while rejecting backgrounds. Because $\gtrsim 100$ TeV neutrinos are absorbed by the Earth [31], EHE ν s are expected to be downgoing or horizontal at IceCube. The dominant background is downgoing atmospheric muon bundles produced in cosmic-ray air showers. This flux is modeled using CORSIKA [32], with SIBYLL2.3c [33] as the hadronic interaction model and the cosmic-ray flux prediction from [34]. Further backgrounds arise from atmospheric and astrophysical neutrinos. Atmospheric neutrinos are produced by meson decays during cosmic-ray air showers. Their flux is divided into a conventional component [35] originating from pion and kaon decays, and a prompt component [36] produced by heavier, short-lived mesons [37]. All neutrinos — atmospheric, astrophysical, and cosmogenic — are simulated using the JULIET code [38].

The 3 kHz event trigger rate in IceCube is dominated by atmospheric muons, while the cosmogenic neutrino flux is already constrained to $\ll 1$ event/year [23]. The signal-to-noise ratio is improved by employing an event selection based on quality cuts of high-energy events in combination with an IceTop veto. Full details of the event selection are presented in the End Matter. In brief, cosmogenic signal events have extremely high energies and therefore produce large amounts of charge (PE). As the atmospheric muon background is exclusively downgoing, we reject most backgrounds with a zenith-angle-dependent charge threshold. To do this, the event direction is reconstructed with a maximum-likelihood reconstruction using an infinite-length track hypothesis [39].

Energy loss profiles for single muons show large stochastic variations as the muons propagate. In contrast, in high-multiplicity muon bundles, these single muon fluctuations partly average out. To leverage this, the energy loss profile of events is reconstructed along the track direction, and stricter charge requirements are imposed upon less stochastic events. Using stochasticity information improved the effective area by 15% between 100 PeV and 1 EeV relative to the previous search. Lastly, IceTop is used to further reduce the background from atmospheric events, as described in [40]. The sample is divided into sub-samples of tracks and cascades based on the reconstructed particle velocity, and their

deposited energy and arrival direction are reconstructed with likelihood-based methods [41, 42] (cf. End Matter).

After the event selection, the expected atmospheric background is 0.40 ± 0.03 events, and up to ~ 5 cosmogenic neutrinos are expected for the most optimistic model [10], consisting of 73 % tracks and 27 % cascades. The flux beyond PeV energies is not well constrained and the expectation strongly depends on the assumed model. The astrophysical expectation ranges from ~ 9 events for an unbroken power law with a hard spectral index ($\gamma = -2.37$) [43], down to ~ 0.5 events assuming a power law with a cutoff ($\gamma = -2.39$, $E_{\text{cutoff}} = 1.4$ PeV) [44]. These best fit parameters follow from the analysis scheme in [45], and they will be published in future work.

For both astrophysical and cosmogenic neutrinos a flavor ratio of $\nu_e : \nu_\mu : \nu_\tau = 1 : 1 : 1$ at Earth is assumed [46], as well as equal fluxes of neutrinos and antineutrinos.

Three events with PeV energies survive the event selection: a through-going track [43], an un-contained cascade [47], and a starting track [48].

Analysis Method — To infer physics parameters, the data is fit using a binned Poisson likelihood in the space of reconstructed direction and energy, following the method in [23]. The observable binning is adopted from [23], except here 10 directional cascade bins are used [49].

The expectation in each observable bin i is the sum of cosmogenic ($\mu_{\text{GZK},i}$) and astrophysical ($\mu_{\text{astro},i}$) neutrinos, plus all other atmospheric backgrounds ($\mu_{\text{bkg},i}$), and is compared to the number of observed events n_i . The overall normalizations of the cosmogenic and astrophysical models— λ_{GZK} and λ_{astro} —are allowed to float, with the latter a nuisance parameter.

$$\mathcal{L}(\lambda_{\text{GZK}}, \lambda_{\text{astro}}) = \prod_i \text{Pois}(n_i | \lambda_{\text{GZK}} \mu_{\text{GZK},i} + \lambda_{\text{astro}} \mu_{\text{astro},i} + \mu_{\text{bkg},i}). \quad (1)$$

Being in the regime of small statistics, all hypothesis tests are based on ensembles of pseudo-experiments. Confidence intervals are determined using the likelihood ratio test statistic (TS) [50].

The compatibility of a cosmogenic neutrino model with observed data is tested via the likelihood ratio test:

$$\Lambda = \log \left(\frac{\sup_{\lambda_{\text{GZK}}, \lambda_{\text{astro}}} \mathcal{L}(\lambda_{\text{GZK}}, \lambda_{\text{astro}})}{\sup_{\lambda_{\text{astro}}} \mathcal{L}(\lambda_{\text{GZK}} = 1, \lambda_{\text{astro}})} \right), \quad (2)$$

where sup denotes the supremum.

To determine EHE ν flux constraints in a more model-independent manner, a differential upper limit is constructed. For this, a sliding E^{-1} neutrino spectrum extending half a decade to both sides around the central energy is injected in half-decade-wide steps [23]. Here, $\gamma = -1$ is chosen for comparability with previous results and results from other experiments.

When performing hypothesis tests, an astrophysical spectral model is assumed. For model tests, we assume a power-law spectrum with spectral index $\gamma = -2.37 \pm 0.09$ observed in the energy range 15 TeV to 5 PeV [51], where the indicated range is considered as a systematic uncertainty. Furthermore, when constructing pseudo-experiments, a value of the unknown astrophysical flux normalization must be assumed. The value of λ_{astro} used in pseudo-experiments is informed by its best fit obtained from data [52]. This balances model rejection power with the discovery potential for cosmogenic neutrinos, while giving good coverage. However, the differential neutrino limit and the proton fraction constraints are constructed as upper limits, i.e. even in case of an observation incompatible with background, only upper limits are reported. To ensure conservative upper limits, the single power-law model with exponential cutoff [45] is used and pseudo-experiments are performed assuming $\lambda_{\text{astro}} = 0$. Recently, IceCube reported an indication favoring a broken power law for the measured astrophysical flux [45]. However, upper limits are more conservative when a power law with exponential cutoff is used instead. The effect of assuming a softer spectral index ($\gamma = -2.52$ [45]) ranges from -30 % (Murase [53]) to 6 % (van Vliet [20]), and is negligible at the 1 %-level for Ahlers 2010 [10].

Systematic uncertainties are treated similarly to [46]. Since the observed number of events is small, fitting multiple nuisance parameters is unfeasible. Instead, the impact of systematics is estimated by varying them in pseudo-experiments based on estimated priors. This procedure modifies n_i in Eq. 1, widens the distribution of TS values, and thus the extracted confidence intervals. The parameters taken into account are: the optical efficiency of the DOMs (± 10 %) [28], the neutrino cross section ($^{+3}_{-20}$ %) [31, 54], the average neutrino inelasticity (± 20 %) [31, 54], the atmospheric muon flux ($^{+73}_{-46}$ %) and the conventional (± 30 %) [55] and prompt (± 100 %) [36] atmospheric neutrino flux. The uncertainty on the atmospheric muon flux is dominated by composition uncertainties of the cosmic-ray flux at Earth and the range is constructed by re-weighting the simulation to a primary cosmic-ray flux of protons or iron nuclei only [32, 34]. The baseline normalization of the atmospheric muon component is measured from a fit to sub-threshold data. The effect of incorporating systematics is modest, with the differential limit weakened by 4 % at 100 PeV, reducing towards 1 % at the highest energies.

Results — *Differential limit and model tests* — The differential upper limit on the neutrino flux above 5×10^6 GeV is depicted in Fig. 1 as a red line. The sensitivity, i.e., the limit in case of a null observation, is also shown. The limit is weakened with respect to the sensitivity below 100 PeV due to the three observed events. The differential limit is compared to a representative variety of cosmogenic neutrino models as grey lines. Qual-

itatively, larger normalizations, higher maximum accelerating energies, and stronger source evolutions generate larger cosmogenic neutrino fluxes [11, 12, 56]. In contrast, when the injected cosmic-ray primaries are heavy nuclei, photo-disintegration becomes the dominant process over photo-pion production and the neutrino flux is suppressed [6, 13, 57]. All model predictions shown in Fig. 1 (except [20]) assume a pure-proton composition with moderate source redshift evolutions comparable to the SFR. The maximum acceleration energy varies between 10^{11} GeV and 10^{12} GeV.

For each aforementioned model, we performed a likelihood ratio test (Eq. 2). The resulting p-values, and the upper limits at 90% CL are presented in Tab. I. Although three events were observed, the best fit λ_{GZK} for all tested models is zero. This indicates the data can be sufficiently explained by astrophysical neutrinos. All tested cosmogenic models assuming a pure proton composition of UHECRs are rejected at 95% CL. This indicates that regardless of the differences between those models, if the SFR is driving the source evolution of UHECRs, a proton-only composition can be excluded.

Proton fraction constraints — Given the measured UHECR flux, the non-observation of neutrinos imposes constraints on the sources. This approach is complementary to many existing models, which focus on accurately describing the cosmic-ray energy spectrum and composi-

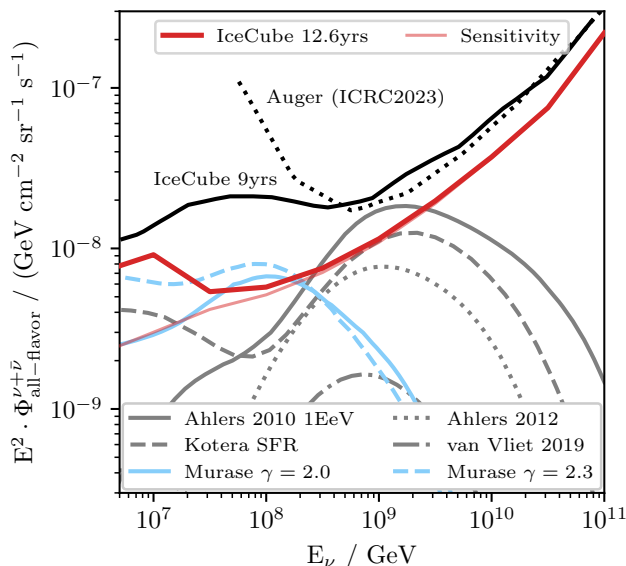


FIG. 1. Differential upper limit (90% CL) on the neutrino flux. The differential limit is compared to the IceCube 9 year result [23], the limit by Auger [58], and cosmogenic neutrino flux models [10, 11, 13, 20] and a UHE astrophysical model [53]. The model from [20] assumes $\gamma = 2.5$, $E_{\text{max}} = 10^{20}$ eV, $m = 3.4$ and a 10% proton fraction. The Auger limit is re-scaled to all-flavor, decade-wide bins for comparison.

TABLE I. A selection of cosmogenic neutrino models, the model rejection factor (MRF [59]) at 90% CL, and associated p-value. The analysis strongly ($p < 0.05$) constrains several previously allowed models of the cosmogenic neutrino flux. Cosmogenic models assuming a proton-only composition are marked with a star.

Model	MRF (90% CL)	p-value
Ahlers 2010* [10] (1 EeV)	0.28	0.003
Ahlers 2012* [13]	0.65	0.043
Kotera SFR* [11]	0.49	0.027
van Vliet [20] ($f_p = 0.1, m = 3.4, \alpha = -2.5$)	2.72	0.268
Murase AGN [53] ($\gamma = -2.0, \xi_{\text{CR}} = 3$)	0.47	0.057
Murase AGN [53] ($\gamma = -2.3, \xi_{\text{CR}} = 100$)	0.62	0.019

tion, and thus also obtain an estimation of the accompanying cosmogenic neutrino flux [15, 19, 60, 61].

The CRPropa package [62] is used to model cosmogenic fluxes (following [20]). In the simulation, protons and secondary neutrinos are propagated to Earth including energy losses from photo-pion production and pair production on the CMB and EBL [63], neutron decay and cosmological adiabatic losses. Identical sources are distributed homogeneously and isotropically with a power-law injection spectrum ($\Phi(E) \propto E^\alpha \exp(-E/E_{\text{max}})$) with spectral index $\alpha \in [-1.0, -3.0]$ and exponential cut-off at $E_{\text{max}} \in [4 \times 10^{10} \text{ GeV}, 10^{14} \text{ GeV}]$. Two different models for cosmological source evolution are tested

$$\text{SE}_1(z) = \begin{cases} (1+z)^m, & z \leq z' \\ (1+z')^m, & z > z' \end{cases} \quad (3)$$

with $z' = 1.5$ up to $z_{\text{max}} = 4$ [20], and a more conservative model of $\text{SE}_2(z) = (1+z)^m$ with $z_{\text{max}} = 2$, where m denotes the source evolution parameter. The simulation is normalized to the all-particle cosmic-ray flux measured by Auger at $10^{10.55}$ GeV [64]. We normalize to the highest energy data point below the observed GZK-suppression, such that the cosmic-ray flux at the suppression energy is saturated. This defines the flux corresponding to a proton fraction at Earth (f_p) of 100% above energies of $\simeq 30$ EeV.

Fig. 2 shows the construction of the f_p constraints [65]. The light-colored histograms show the simulated proton flux saturating the Auger measurement and the secondary neutrino flux. The source parameters α and E_{max} are chosen to minimize the integral neutrino energy flux to obtain a conservative prediction for a given value of m . The flux shown in the figure is in tension with IceCube data, and thus f_p can be constrained based on the determined upper limit.

This procedure is repeated for different values of the source evolution parameter m , and the resulting constraints are shown in Fig. 3 for the source evolution

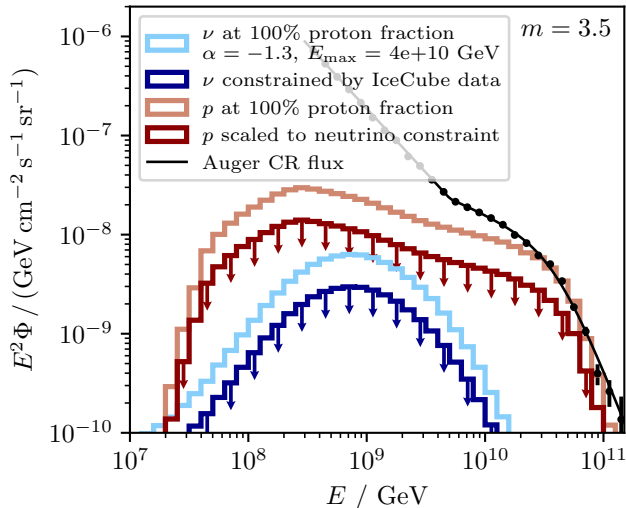


FIG. 2. Illustration of the construction of proton fraction constraints. The red and blue histograms are 90% CL upper limits on the flux of UHECR protons and cosmogenic neutrinos (per-flavor), derived from the non-observation of EHE ν , assuming $SE_1(z)$ with $m = 3.5$. Also plotted in black is the cosmic-ray flux measured by Auger [66]. The light-colored histograms represent the case where the proton flux (light-red) is allowed to saturate the Auger measurement at $10^{10.55}$ GeV. The corresponding neutrino flux (light-blue) is in tension with the non-observation in IceCube data, and is therefore excluded.

models $SE_1(z)$ and $SE_2(z)$ [67]. For instance, given the source evolution is comparable to the SFR or stronger, f_p is constrained to be below about 70%. This is the first direct confirmation by neutrino data that the composition of UHECRs at energies above 30 EeV is not pure protons, as already seen in Auger’s X_{\max} measurements [25] and TA’s isotropy data [26]. Alternatively, due to the degeneracy between f_p and m , the results can be interpreted as an upper bound on the source evolution of $m \lesssim 3$ for proton-dominated UHECRs, strengthening the claim of the previous analysis [40]. Notably, the method used in this study does not rely on observables from air showers and is therefore insensitive to the uncertainties associated with hadronic interaction models [68]. This makes the measurement a complementary confirmation of the composition measurements based on observables derived from air showers.

The predicted neutrino fluxes are dominated by distant cosmic-ray sources, from which high-energy cosmic rays are not expected to survive. The model presented here assumes that cosmic-ray sources are distributed homogeneously within the universe. This is true at large distances, but due to Earth’s position within the Local Supercluster and Local Sheet, the local density of sources is enhanced. This leads to a relative reduction of distant sources and thus of the expected neutrino flux. Including

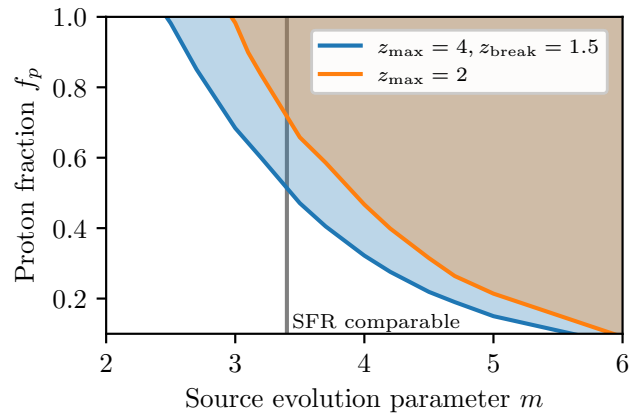


FIG. 3. Constraints on the proton fraction (f_p) of UHECRs as a function of source evolution parameter m at 90% CL based on the non-observation of UHE neutrinos in this study. The excluded region is shown for the two source evolution models $SE_1(z)$ (blue) and $SE_2(z)$ (orange).

a model of the local overdensity of sources based on the star formation rate of local galaxies [25, 69] weakens the neutrino fluxes, and the corresponding proton fraction constraints, by about 3% ($m = 6.0$) to 4% ($m = 2.0$). Additionally, a recent study from Auger shows that up to 5% of UHECRs above 40 EeV can be associated with Centaurus A as the dominant local source [70]; in this case, the f_p constraint becomes weaker by the same fraction.

AGN model constraints — In addition, we tested the active-galactic-nuclei (AGN) model from [53], instead of a cosmogenic flux model. The astrophysical neutrino flux described in this model cannot be explained by the observed sub-PeV astrophysical neutrinos (cf. Fig. 1). These UHE astrophysical neutrinos are indistinguishable from cosmogenic neutrinos event-by-event. The neutrino emission is based on observed photon fluxes, using phenomenological parameters like the cosmic-ray loading factor ξ_{CR} . The modeled flux scales linearly with ξ_{CR} , so the limit (cf. Tab. I) can be interpreted as an upper limit of $\xi_{CR} \leq 1.4$ and $\xi_{CR} \leq 62$ for assumed CR spectral indexes of $\gamma = 2.0$ and 2.3, respectively. That the resulting MRFs are < 1 indicates that inner jets of AGN are unlikely to be a dominant source for UHECRs in this model scenario.

Summary — The non-observation of neutrinos with energies well above 10 PeV in 12.6 years of IceCube data places the most stringent limit on cosmogenic neutrino fluxes to date, reaching a neutrino flux of $E^2\Phi_{\nu_e+\nu_\mu+\nu_\tau} \simeq 10^{-8} \text{ GeV cm}^{-2} \text{ s}^{-1} \text{ sr}^{-1}$. Additionally, we provide the strongest constraints on the composition of UHECRs obtained by neutrino astronomy, disfavoring proton-only UHECRs if their sources are evolving with the SFR or stronger.

The IceCube Collaboration acknowledges the signifi-

cant contributions to this manuscript by Brian A. Clark and Maximilian Meier. The authors gratefully acknowledge the support from the following agencies and institutions: USA – U.S. National Science Foundation-Office of Polar Programs, U.S. National Science Foundation-Physics Division, U.S. National Science Foundation-EPSCoR, U.S. National Science Foundation-Office of Advanced Cyberinfrastructure, Wisconsin Alumni Research Foundation, Center for High Throughput Computing (CHTC) at the University of Wisconsin–Madison, Open Science Grid (OSG), Partnership to Advance Throughput Computing (PATH), Advanced Cyberinfrastructure Coordination Ecosystem: Services & Support (ACCESS), Frontera and Ranch computing project at the Texas Advanced Computing Center, U.S. Department of Energy-National Energy Research Scientific Computing Center, Particle astrophysics research computing center at the University of Maryland, Institute for Cyber-Enabled Research at Michigan State University, Astroparticle physics computational facility at Marquette University, NVIDIA Corporation, and Google Cloud Platform; Belgium – Funds for Scientific Research (FRS-FNRS and FWO), FWO Odysseus and Big Science programmes, and Belgian Federal Science Policy Office (Belspo); Germany – Bundesministerium für Bildung und Forschung (BMBF), Deutsche Forschungsgemeinschaft (DFG), Helmholtz Alliance for Astroparticle Physics (HAP), Initiative and Networking Fund of the Helmholtz Association, Deutsches Elektronen Synchrotron (DESY), and High Performance Computing cluster of the RWTH Aachen; Sweden – Swedish Research Council, Swedish Polar Research Secretariat, Swedish National Infrastructure for Computing (SNIC), and Knut and Alice Wallenberg Foundation; European Union – EGI Advanced Computing for research; Australia – Australian Research Council; Canada – Natural Sciences and Engineering Research Council of Canada, Calcul Québec, Compute Ontario, Canada Foundation for Innovation, WestGrid, and Digital Research Alliance of Canada; Denmark – Vilum Fonden, Carlsberg Foundation, and European Commission; New Zealand – Marsden Fund; Japan – Japan Society for Promotion of Science (JSPS) and Institute for Global Prominent Research (IGPR) of Chiba University; Korea – National Research Foundation of Korea (NRF); Switzerland – Swiss National Science Foundation (SNSF).

* also at Institute of Physics, Sachivalaya Marg, Sainik School Post, Bhubaneswar 751005, India

† also at Department of Space, Earth and Environment, Chalmers University of Technology, 412 96 Gothenburg, Sweden

‡ also at Earthquake Research Institute, University of Tokyo, Bunkyo, Tokyo 113-0032, Japan

- [1] Particle Data Group, Review of particle physics, *Prog. Theor. Exp. Phys.* **2020**, 083C01 (2020).
- [2] M. Ahlers, High-energy Cosmogenic Neutrinos, *Phys. Procedia* **61**, 392 (2015).
- [3] V. Berezhinsky and G. Zatsepin, Cosmic rays at ultrahigh-energies (neutrino?), *Phys. Lett. B* **28**, 423 (1969).
- [4] C. T. Hill and D. N. Schramm, Ultrahigh-Energy Cosmic Ray Neutrinos, *Phys. Lett. B* **131**, 247 (1983).
- [5] R. Engel, D. Seckel, and T. Stanev, Neutrinos from propagation of ultrahigh-energy protons, *Phys. Rev. D* **64**, 093010 (2001).
- [6] D. Hooper, A. Taylor, and S. Sarkar, The Impact of heavy nuclei on the cosmogenic neutrino flux, *Astropart. Phys.* **23**, 11 (2005).
- [7] L. A. Anchordoqui, H. Goldberg, D. Hooper, S. Sarkar, and A. M. Taylor, Predictions for the Cosmogenic Neutrino Flux in Light of New Data from the Pierre Auger Observatory, *Phys. Rev. D* **76**, 123008 (2007).
- [8] H. Takami, K. Murase, S. Nagataki, and K. Sato, Cosmogenic neutrinos as a probe of the transition from Galactic to extragalactic cosmic rays, *Astropart. Phys.* **31**, 201 (2009).
- [9] M. Ahlers, L. A. Anchordoqui, and S. Sarkar, Neutrino diagnostics of ultra-high energy cosmic ray protons, *Phys. Rev. D* **79**, 083009 (2009).
- [10] M. Ahlers, L. Anchordoqui, M. Gonzalez-Garcia, F. Halzen, and S. Sarkar, GZK neutrinos after the Fermi-LAT diffuse photon flux measurement, *Astropart. Phys.* **34**, 106–115 (2010).
- [11] K. Kotera, D. Allard, and A. V. Olinto, Cosmogenic Neutrinos: parameter space and detectability from PeV to ZeV, *JCAP* **2010** (10), 013.
- [12] S. Yoshida and A. Ishihara, Constraints on the origin of the ultra-high energy cosmic-rays using cosmic diffuse neutrino flux limits: An analytical approach, *Phys. Rev. D* **85**, 063002 (2012).
- [13] M. Ahlers and F. Halzen, Minimal cosmogenic neutrinos, *Phys. Rev. D* **86**, 083010 (2012).
- [14] R. Aloisio, D. Boncioli, A. di Matteo, A. F. Grillo, S. Petrerà, and F. Salamida, Cosmogenic neutrinos and ultrahigh energy cosmic ray models, *JCAP* **2015** (10), 006.
- [15] J. Heinze, D. Boncioli, M. Bustamante, and W. Winter, Cosmogenic neutrinos challenge the cosmic-ray proton dip model, *ApJ* **825**, 122 (2016).
- [16] A. Romero-Wolf and M. Ave, Bayesian Inference Constraints on Astrophysical Production of Ultra-high Energy Cosmic Rays and Cosmogenic Neutrino Flux Predictions, *JCAP* **2018** (07), 025.
- [17] R. Alves Batista, R. M. de Almeida, B. Lago, and K. Kotera, Cosmogenic photon and neutrino fluxes in the Auger era, *JCAP* **2019** (01), 002.
- [18] J. Heinze, A. Fedynitch, D. Boncioli, and W. Winter, A new view on Auger data and cosmogenic neutrinos in light of different nuclear disintegration and air-shower models, *ApJ* **873**, 88 (2019).
- [19] K. Möller, P. B. Denton, and I. Tamborra, Cosmogenic neutrinos through the grand lens unveil the nature of cosmic accelerators, *JCAP* **2019** (05), 047.
- [20] A. van Vliet, R. A. Batista, and J. R. Hörandel, Determining the fraction of cosmic-ray protons at ultrahigh energies with cosmogenic neutrinos, *Phys. Rev. D* **100**, 021302 (2019).
- [21] K. Greisen, End to the cosmic-ray spectrum?, *Phys. Rev. Lett.* **16**, 748 (1966).

- [22] G. T. Zatsepin and V. A. Kuz'min, Upper Limit of the Spectrum of Cosmic Rays, *Soviet JETP Letters* **4**, 78 (1966).
- [23] M. Aartsen *et al.*, Differential limit on the extremely-high-energy cosmic neutrino flux in the presence of astrophysical background from nine years of IceCube data, *Phys. Rev. D* **98**, 062003 (2018).
- [24] A. Aab *et al.*, Probing the origin of ultra-high-energy cosmic rays with neutrinos in the EeV energy range using the Pierre Auger Observatory, *JCAP* **2019** (10), 022.
- [25] A. Abdul Halim *et al.*, Constraining the sources of ultra-high-energy cosmic rays across and above the ankle with the spectrum and composition data measured at the Pierre Auger Observatory, *JCAP* **2023** (05), 024.
- [26] R. U. Abbasi *et al.*, Isotropy of cosmic rays beyond 10^{20} eV favors their heavy mass composition, *Phys. Rev. Lett.* **133**, 041001 (2024).
- [27] M. Aartsen *et al.*, The IceCube Neutrino Observatory: instrumentation and online systems, *JINST* **12** (03), P03012 (2017).
- [28] R. Abbasi *et al.*, Calibration and characterization of the icecube photomultiplier tube, *Nucl. Instrum. Methods Phys. Res. A* **618**, 139–152 (2010).
- [29] R. Abbasi *et al.*, The IceCube data acquisition system: Signal capture, digitization, and timestamping, *Nucl. Instrum. Methods Phys. Res. A* **601**, 294–316 (2009).
- [30] R. Abbasi *et al.*, IceTop: The surface component of IceCube, *Nucl. Instrum. Methods Phys. Res. A* **700**, 188–220 (2013).
- [31] A. Cooper-Sarkar, P. Mertsch, and S. Sarkar, The high energy neutrino cross-section in the Standard Model and its uncertainty, *JHEP* **2011** (8), 042.
- [32] D. Heck, J. Knapp, J. N. Capdevielle, G. Schatz, and T. Thouw, CORSIKA: A Monte Carlo code to simulate extensive air showers, (1998).
- [33] A. Fedynitch, F. Riehn, R. Engel, T. K. Gaisser, and T. Stanev, Hadronic interaction model sibyll 2.3c and inclusive lepton fluxes, *Phys. Rev. D* **100**, 103018 (2019).
- [34] T. K. Gaisser, Spectrum of cosmic-ray nucleons, kaon production, and the atmospheric muon charge ratio, *Astropart. Phys.* **35**, 801–806 (2012).
- [35] M. Honda, T. Kajita, K. Kasahara, S. Midorikawa, and T. Sanuki, Calculation of atmospheric neutrino flux using the interaction model calibrated with atmospheric muon data, *Phys. Rev. D* **75**, 043006 (2007).
- [36] A. Bhattacharya, R. Enberg, M. H. Reno, I. Sarcevic, and A. Stasto, Perturbative charm production and the prompt atmospheric neutrino flux in light of RHIC and LHC, *JHEP* **2015** (6), 110.
- [37] The latter has yet to be observed experimentally [51].
- [38] S. Yoshida, R. Ishibashi, and H. Miyamoto, Propagation of extremely high energy leptons in Earth: Implications for their detection by the IceCube neutrino telescope, *Phys. Rev. D* **69**, 103004 (2004).
- [39] K. Schatto, *Stacked searches for high-energy neutrinos from blazars with IceCube*, Ph.D. thesis, Mainz (2014).
- [40] M. G. Aartsen *et al.*, Constraints on Ultrahigh-Energy Cosmic-Ray Sources from a Search for Neutrinos above 10 PeV with IceCube, *Phys. Rev. Lett.* **117**, 241101 (2016).
- [41] M. G. Aartsen *et al.*, Energy reconstruction methods in the IceCube neutrino telescope, *JINST* **9** (03), P03009 (2014).
- [42] R. Abbasi *et al.*, Improved modeling of in-ice particle showers for IceCube event reconstruction, *JINST* **19** (06), P06026 (2024).
- [43] M. G. Aartsen *et al.*, Observation and Characterization of a Cosmic Muon Neutrino Flux from the Northern Hemisphere using six years of IceCube data, *ApJ* **833**, 3 (2016).
- [44] At the highest energies, $E_\nu > 100$ PeV, this expectation is reduced to 0.9 events and 3×10^{-30} events respectively.
- [45] R. Naab, E. Ganster, and Z. Zhang, Measurement of the astrophysical diffuse neutrino flux in a combined fit of IceCube's high energy neutrino data, *PoS ICRC2023*, 1064 (2023).
- [46] R. Abbasi *et al.*, Observation of Seven Astrophysical Tau Neutrino Candidates with IceCube, *Phys. Rev. Lett.* **132**, 151001 (2024).
- [47] M. G. Aartsen *et al.*, Detection of a particle shower at the Glashow resonance with IceCube, *Nature* **591**, 220–224 (2021).
- [48] IceCube Collaboration, GCN Circular 24028, GRB Coordinates Network (2019), gcn.nasa.gov/circulars/24028.
- [49] The cascade angular binning is guided by the resolution of recent reconstruction algorithms [42].
- [50] G. J. Feldman and R. D. Cousins, Unified approach to the classical statistical analysis of small signals, *Phys. Rev. D* **57**, 3873 (1998).
- [51] R. Abbasi *et al.*, Improved Characterization of the Astrophysical Muon–neutrino Flux with 9.5 Years of IceCube Data, *ApJ* **928**, 50 (2022).
- [52] M. A. Acero *et al.*, The Profiled Feldman-Cousins technique for confidence interval construction in the presence of nuisance parameters (2022), [arXiv:2207.14353](https://arxiv.org/abs/2207.14353).
- [53] K. Murase, Y. Inoue, and C. D. Dermer, Diffuse neutrino intensity from the inner jets of active galactic nuclei: Impacts of external photon fields and the blazar sequence, *Phys. Rev. D* **90**, 023007 (2014).
- [54] K. Xie, J. Gao, T. Hobbs, D. R. Stump, and C.-P. Yuan, High-energy neutrino deep inelastic scattering cross sections, *Phys. Rev. D* **109**, 113001 (2024).
- [55] J. P. Yañez and A. Fedynitch, Data-driven muon-calibrated neutrino flux, *Phys. Rev. D* **107**, 123037 (2023).
- [56] G. Decerprit and D. Allard, Constraints on the origin of ultrahigh energy cosmic rays from cosmogenic neutrinos and photons, *Astron. Astrophys.* **535**, A66 (2011).
- [57] M. Ave, N. Busca, A. Olinto, A. Watson, and T. Yamamoto, Cosmogenic neutrinos from ultra-high energy nuclei, *Astropart. Phys.* **23**, 19–29 (2005).
- [58] M. Niechciol *et al.*, Latest results from the searches for ultra-high-energy photons and neutrinos at the Pierre Auger Observatory, *PoS ICRC2023*, 1488 (2023).
- [59] G. C. Hill and K. Rawlins, Unbiased cut selection for optimal upper limits in neutrino detectors: the model rejection potential technique, *Astropart. Phys.* **19**, 393–402 (2003).
- [60] M. S. Muzio, M. Unger, and S. Wissel, Prospects for joint cosmic ray and neutrino constraints on the evolution of trans-Greisen-Zatsepin-Kuzmin proton sources, *Phys. Rev. D* **107**, 103030 (2023).
- [61] D. Ehlert, A. van Vliet, F. Oikonomou, and W. Winter, Constraints on the proton fraction of cosmic rays at the highest energies and the consequences for cosmogenic neutrinos and photons, *JCAP* **2024** (02), 022.
- [62] R. Alves Batista *et al.*, CRPropa 3.2 — an advanced framework for high-energy particle propagation in extra-

- galactic and galactic spaces, JCAP **2022** (09), 035.
- [63] A. Franceschini, G. Rodighiero, and M. Vaccari, Extragalactic optical-infrared background radiation, its time evolution and the cosmic photon-photon opacity, *Astron. Astrophys.* **487**, 837–852 (2008).
- [64] The reference energy impacts the resulting neutrino fluxes. A systematic shift to the reference energy on the order of the systematic energy scale of Auger of $\pm 14\%$ [25] results in a 5% shift of the overall neutrino flux.
- [65] As suggested in [20], f_p can be determined by comparing the predicted neutrino flux with the experimental limit at 1 EeV. However, we instead perform a model test, which improves the sensitivity to the cosmogenic flux, even when choosing conservative source parameters.
- [66] F. Fenu *et al.*, The cosmic ray energy spectrum measured using the Pierre Auger Observatory, PoS **ICRC2017**, 486 (2018).
- [67] The value of m for UHECR sources is unknown. Here, we focus on the range in which f_p can be constrained by this analysis.
- [68] Technically, the estimation of the atmospheric muon/neutrino background has a dependence on hadronic interaction models, but the influence on the derived constraints is negligible.
- [69] J. Biteau, Stellar Mass and Star Formation Rate within a Billion Light-years, *ApJ Supplement Series* **256**, 15 (2021).
- [70] A. A. Halim *et al.*, Constraining models for the origin of ultra-high-energy cosmic rays with a novel combined analysis of arrival directions, spectrum, and composition data measured at the Pierre Auger Observatory, JCAP **2024** (01), 022.
- [71] R. Abbasi *et al.*, First search for extremely high energy cosmogenic neutrinos with the IceCube Neutrino Observatory, *Phys. Rev. D* **82**, 072003 (2010).
- [72] M. Dunsch *et al.*, Recent improvements for the lepton propagator PROPOSAL, *Comput. Phys. Commun.* **242**, 132 (2019).
- [73] D. Chirkin, J. C. Díaz-Vélez, C. Kopper, A. Olivas, B. Riedel, M. Rongen, D. Schultz, and J. van Santen, Photon Propagation using GPUs by the IceCube Neutrino Observatory, in *2019 15th International Conference on eScience (eScience)* (2019) pp. 388–393.
- [74] J. Lundberg, P. Miočinović, K. Woschnagg, T. Burgess, J. Adams, S. Hundertmark, P. Desiati, and P. Niessen, Light tracking through ice and water—Scattering and absorption in heterogeneous media with Photonics, *Nucl. Instrum. Methods Phys. Res. A* **581**, 619 (2007).
- [75] L. D. Landau and I. I. Pomeranchuk, The limits of applicability of the theory of Bremsstrahlung by electrons and of the creation of pairs at large energies, *Dokl. Akad. Nauk SSSR* **92**, 535 (1953).
- [76] A. B. Migdal, Bremsstrahlung and pair production in condensed media at high-energies, *Phys. Rev.* **103**, 1811 (1956).
- [77] L. Gerhardt and S. R. Klein, Electron and Photon Interactions in the Regime of Strong LPM Suppression, *Phys. Rev. D* **82**, 074017 (2010).

TABLE II. For the four analysis cuts, the table describes the number of atmospheric muons, atmospheric neutrinos, and astrophysical neutrinos [51] passing the cuts. The final column provides a cosmogenic neutrino flux prediction [10].

Cut Stage	Atm μ	Atm ν	Astro ν	Cosmo ν
(1) Charge & Hit Cut	5.5×10^4	4.8	37	11.5
(2) Track Quality Cut	8.2×10^3	0.4	1.3	8.5
(3) Muon Bundle Cut	0.6	0.2	0.5	5.6
(4) IceTop Veto	0.2	0.2	0.5	5.4

Event Selection: The event selection approach is based on a previous IceCube study [40], where signal candidates are found by applying four consecutive steps that are designed to remove atmospheric and astrophysical backgrounds. Tab. II provides the expected number of background events passing each cut stage, along with the expectation for a cosmogenic neutrino flux [10].

In the first step of the event selection, only events with a total recorded charge of $Q_{\text{tot}} \geq 27\,500$ PE and a number of hit DOMs of $n_{\text{DOMs}} \geq 100$ are kept. This cut already rejects a majority of atmospheric neutrinos, reducing the expected background to < 10 events.

The second step of the event selection is shown as the grey line in Fig. 4. The cut is a two-dimensional cut in the plane of reconstructed relative particle velocity $\beta = |\vec{v}|/c$ and the total recorded charge Q_{tot} . Mathematically,

$$\log_{10} \left(\frac{Q_{\text{tot}}}{\text{PE}} \right) > \begin{cases} 5.33 & \beta \leq 0.867 \\ 5.33 - 30(\beta - 0.867) & 0.867 < \beta \leq 0.934 \\ 4.73 & \beta > 0.934. \end{cases} \quad (4)$$

The cut has multiple purposes. It rejects atmospheric neutrinos, and also rejects mis-reconstructed atmospheric muon events and neutrino events. The speed is reconstructed with the “LineFit” algorithm [71], which assumes a light source traveling with a velocity \vec{v} along an infinite-length track. For a well-reconstructed track the speed will be distributed around the speed of light ($|\vec{v}| \simeq c \simeq 0.3 \text{ m ns}^{-1}$). (Apparently “super-luminal” tracks are also possible due to uncertainty of the reconstruction.) At this stage, 65% of signal events are tracks well reconstructed with β within 10% of c , and the majority of outliers are cascades with $\beta < 0.9$. As a consequence, the speed can also be used to separate the final event sample into subsets of cascades and tracks, which is done at $|\vec{v}| = 0.27 \text{ m ns}^{-1}$, shown as a vertical dashed line in Figure 4. The design of the event selection is mainly motivated by the distribution of the dominant track-like events but is applied in the same fashion to all events, including cascades. After the track quality cut, the atmospheric neutrino expectation is < 1 . After this cut stage, the sample is dominated by downgoing atmospheric muon bundles. Therefore, at this stage in the analysis, we use a one-dimensional fit in observed charge

between $5 \times 10^4 - 10^6$ PE to determine the overall normalization of the atmospheric muon flux.

The third step of the event selection is designed to remove the main background of down-going muon bundles. The cut is made in the 2D-plane of reconstructed particle zenith $\cos(\theta)$ and total recorded charge Q_{tot} and is visible in Fig. 5. In this plane, the differences between signal (cosmogenic neutrinos) and dominant background (atmospheric muons) appears in both the zenith distribution and the energy loss profile of single muons/taus compared to muon bundles with large muon multiplicities. As the energy of a muon increases, its energy losses become more stochastic. In a muon bundle with the same total energy, the energy is distributed among many muons, resulting in a superposition of lower energy muons losing their energy more continuously, even though their mean dE/dx is comparable. To obtain a measure of the “stochasticity” of an event, the energy loss profile is reconstructed using a segmented energy loss reconstruction [41] over a distance of 40 m. The reconstructed loss profile is then compared to a muon bundle PDF obtained with PROPOSAL [72]. The PDF is determined by simulating muon bundles for 40 m repeatedly and recording their total energy loss. Then, we define the reconstructed stochasticity: $\kappa = -\sum_i \log(P(\Delta E_i/E))/\text{ndf}$, where the sum runs over all unfolded energy depositions ΔE_i in the reconstruction, and $\Delta E_i/E$ are the relative energy losses of the event. This produces a variable comparable to a reduced log-likelihood, the distribution of which is shown for atmospheric muon bundles and single high-energy muons in Figure 6. Events with $\kappa > 8.37$ are regarded as “highly” stochastic.

With the goal of removing downgoing muon bundles, the cut imposes a stronger requirement on downgoing events than upgoing events. The cut is defined by two charge thresholds (a, b), a shape parameter c , and a transition point from the upgoing to downgoing region d :

$$\log_{10} \left(\frac{Q_{\text{tot}}}{\text{PE}} \right) > \begin{cases} a & \cos(\theta) < d \\ a + b\sqrt{1 - \left(\frac{1 - \cos(\theta)}{1 - d}\right)^c} & \cos(\theta) \geq d \end{cases} \quad (5)$$

Parameters values are chosen to maximize the model rejection factor for the cosmogenic neutrino flux prediction in [10]. The final parameter values are $a = 4.777, b = 1.55, c = 1.5, d = 0.12$ for the low stochasticity events, and $a = 4.727, b = 1.05, c = 4, d = 0.10$ for high stochasticity events. The result is a substantially looser selection for highly stochastic downgoing events, as seen in Figure 5. This use of a stochasticity variable is new to this event selection, and improves the MRF by more than 10% relative to the previous event selection.

The fourth and final stage in the event selection uses IceTop to reject atmospheric muons. IceTop hits correlated with an event in the in-ice detector can be found by extrapolating the reconstructed track to the surface and

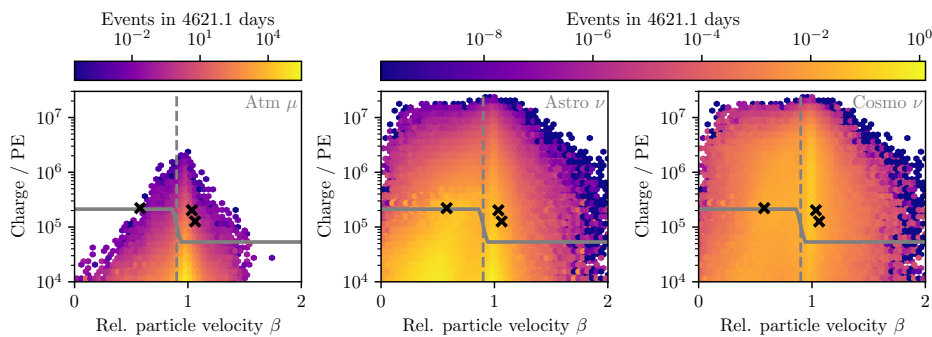


FIG. 4. 2D histograms of the second stage of the event selection. Distribution of charge vs reconstructed relative particle velocity β for atmospheric muons (left), astrophysical neutrinos (center, [51]), and cosmogenic neutrinos (right, [10]). The cut applied is shown as a grey dashed line. The three candidate events passing all cuts are shown as black crosses.

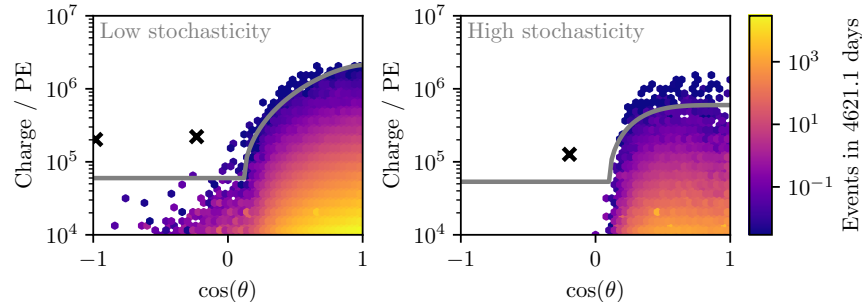


FIG. 5. A 2D histogram showing the third stage of the event selection. Both plots show the distribution of charge as a function of reconstructed zenith for atmospheric muons, with the left panel showing low-stochasticity events, and the right panel showing high stochasticity events. The three candidate events passing all cuts are shown as black crosses.

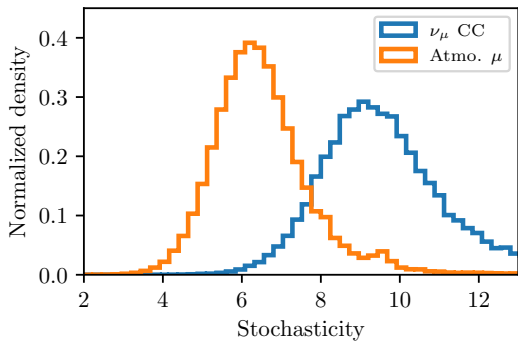


FIG. 6. Distribution of stochasticity for atmospheric muons (muon bundles) and ν_μ CC (single muons) events.

finding the time t_{CA} , where the track is at its closest approach to IceTop. Correlated IceTop hits are defined by the collections of hits that satisfy $-1 \mu\text{s} \leq t_{CA} \leq 1.5 \mu\text{s}$. Events are vetoed if they have two or more correlated hits in IceTop, reducing the remaining atmospheric muon background by $\sim 60\%$ but only reducing the all-sky neutrino rate by $< 5\%$.

The final zenith-averaged neutrino effective area for the event selection (before applying the IceTop veto) is shown in Fig. 7 and compared to the previous version of the event selection [40]. The effective area describes the neutrino-antineutrino average. The new event selection mostly improves the ν_μ effective area between 10 PeV and 1 EeV by about 30%, while reducing the ν_e and ν_τ effective area between 1 PeV and 10 PeV to reduce the background of astrophysical neutrinos.

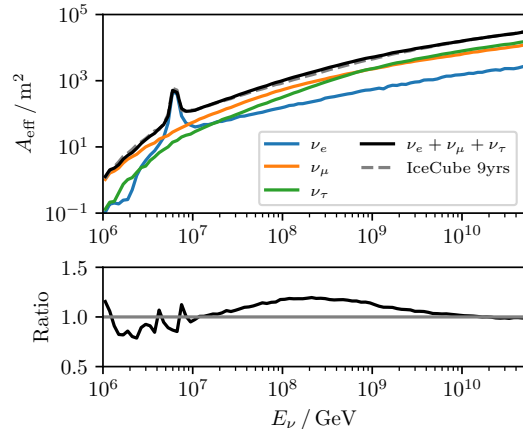


FIG. 7. The sky-averaged effective area of the analysis as a function of energy. The effective area from the previous iteration of this analysis [23] is plotted as dashed line.

Simulation of EHE ν s in IceCube: Simulation of EHE ν s using the conventional IceCube method of ray-tracing individual photons [73] is computationally infeasible. Instead, pre-calculated photon tables are used [74] to reduce the computational cost. The baseline simulation does not include the Landau-Pomeranchuk-Migdal (LPM) effect [75–77]. The scale of the effect was investigated by a special ν_e simulation including the LPM cascade elongation, and the effect was found to be a sub-percent effect on the total event rate of the EHE ν sample used in this work. The LPM effect on π^0 -production in hadronic showers was not tested here.